

Localization and hopping conduction in glass and crystal phases of monatomic Au layers on a silicon surface

Shiro Yamazaki,^{*} Iwao Matsuda,[†] Hiroyuki Okino, Harumo Morikawa,[‡] and Shuji Hasegawa
Department of Physics, School of Science, University of Tokyo, 7-3-1 Hongo, Bunkyo-ku, Tokyo 113-0033, Japan
 (Received 23 June 2008; revised manuscript received 1 December 2008; published 27 February 2009)

Monatomic layers of Au on Si(111) exhibit a glass-crystal phase transition between the ordered crystalline 6×6 reconstruction and the disordered glassy $\beta\text{-}\sqrt{3}\times\sqrt{3}$ reconstruction on thermal annealing. Micro-four-point-probe electrical conductivity measurements clearly revealed that both monatomic layers had conductivities as large as the minimum metallic conductivity at the low-temperature region ($\sim 10\text{--}100$ K), and were well described by transport theory regarding Anderson localization. The sheet conductivity of the 6×6 was higher than that of the $\beta\text{-}\sqrt{3}\times\sqrt{3}$, which was attributed to different degrees of carrier localization.

DOI: [10.1103/PhysRevB.79.085317](https://doi.org/10.1103/PhysRevB.79.085317)

PACS number(s): 73.20.-r, 73.25.+i, 73.63.-b

I. INTRODUCTION

Self-organized systems such as quantum dots, carbon nanotubes, and surface superstructures are key components in the fields of nanoscience and nanotechnology. Electrical transport in these atomic-scale low-dimensional systems is affected much more by atomic disorder and defects than in three-dimensional bulk materials. A large number of studies on electronic transport in disordered thin films have been performed, and theories regarding Anderson localization¹⁻³ and hopping conduction^{4,5} are well established.

Despite intensive investigations on surface superstructures with a diversity of surface science techniques, local electrical conductivity measurements on surfaces have only become feasible in the last ten years. The development of advanced experimental techniques such as the micro-four-point-probe (μ 4PP) method now make direct measurements of the conductivity of surface superstructures possible.⁶⁻⁸ The studies reveal intriguing transport phenomena in monatomic-layer films on crystal surfaces:⁹⁻¹⁴ for example, atomic-scale defects such as atomic steps¹¹ and adatoms¹⁰ significantly affect the surface conductivity.

We report here a transport study on a Au monatomic layer deposited on a Si(111) surface for two different surface reconstructions. By controlled thermal annealing it is possible to modify the disorder in the atomic arrangement of the surface atoms. The disorder in the surface superstructure was found to reduce the magnitude of the conductivity due to carrier localization. In addition, the monatomic layers exhibited conductivities as large as the minimum metallic conductivity at the low-temperature region.

II. EXPERIMENT AND ANALYSIS

The conductivity was measured with μ 4PP chips with a probe spacing of $20\ \mu\text{m}$,⁶ at temperatures (T) ranging from room temperature (RT) to 10 K, in an ultrahigh-vacuum (UHV) chamber equipped with a reflection-high-energy electron-diffraction (RHEED) system.⁶⁻⁸ The voltage drop V was measured between the inner pair of probes while the current I ($\pm 1\text{--}\pm 10\ \mu\text{A}$ depending on T) was supplied via the outer probes on the μ 4PP chip. The slope of the linear I - V curves give the four-point-probe (4PP) resistance R ,

which was converted to the sheet conductivity σ using $\sigma = \ln 2 / (\pi R)$.¹³ The sample temperature was measured by two pairs of gold-iron/chromel thermocouples attached close to the sample. The measurements were performed with decreasing temperature, keeping contact between the probes and sample. To avoid the possible modification of the contact condition due to thermal drift, the probes were retracted and reapproached about every ten measurement points. The scanning tunneling microscope (STM) images were recorded with a commercial STM (UNISOKU Type USM 501) in a separate UHV chamber using the same sample preparation procedures. The Si(111) substrate was n -type (P-doped) with $1\text{--}10\ \Omega\ \text{cm}$ resistivity at RT. The clean Si(111)- 7×7 reconstructed surface was first prepared by direct current heating and Au was deposited on it at $700\ ^\circ\text{C}$. The deposition rate was calibrated using the phase diagram of the Au/Si(111) system.¹⁵⁻¹⁷ After deposition, the sample was annealed at $650\ ^\circ\text{C}$ for 5 min and then cooled to RT. The cooling rate and the Au coverage are important parameters that strongly affect the final surface superstructures. The 6×6 phase [Figs. 1(a) and 1(b)] was prepared by depositing one monolayer (ML) or slightly larger than 1 ML, and slowly cooled by reducing the sample heating current down to zero over 30 min. The $\beta\text{-}\sqrt{3}\times\sqrt{3}$ phase ($\beta\text{-}\sqrt{3}$ phase hereafter) [Figs. 1(c) and 1(d)] was prepared at the same Au coverage but quenched by switching off the heating current. The 6×6 and $\beta\text{-}\sqrt{3}$ phases could be reversibly remade from each other by annealing at $650\ ^\circ\text{C}$ for 5 min and subsequently cooling with the appropriate rate. This is a two-dimensional (2D) glass-crystalline transition between the $\beta\text{-}\sqrt{3}$ phase (disordered glassy phase) and the 6×6 phase (ordered crystalline phase).^{15,17} For Au coverages < 0.92 ML the $\beta\text{-}\sqrt{3}$ phase was always formed irrespective of the cooling rate. For comparison, a " 1×1 " surface was fabricated without postannealing by depositing the same amount of Au on a clean 7×7 substrate at RT. This surface exhibited a diffuse " 1×1 " RHEED pattern and did not yield an atomically resolved STM image [Fig. 1(e)].

We estimated conductivities of the surface-space-charge layer of $\beta\text{-}\sqrt{3}$ and 6×6 phases by solving the Poisson equation with parameters derived from their reported bulk band bending,¹⁸⁻²⁰ and found that it was negligibly small compared with the measured conductivity. Furthermore, the band

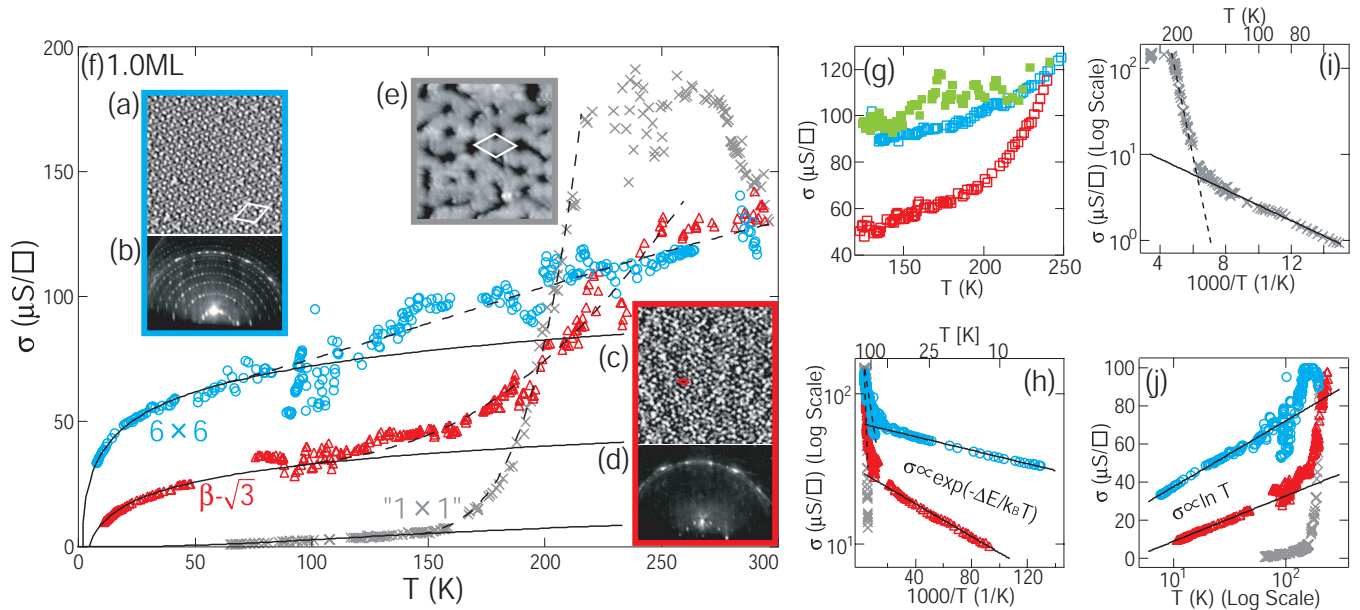


FIG. 1. (Color) (a),(c),(e) Filled-state STM images ($15 \times 15 \text{ nm}^2$) from the Si(111)-Au- 6×6 , $-\beta\sqrt{3}$, and -1×1 samples, respectively. The unit cell of each superstructure is indicated in each image [7×7 unit cell in (e)]. (b) and (d) are RHEED patterns from the 6×6 and $\beta\sqrt{3}$ phases at 10 K. (f) The measured sheet conductivities (σ) as a function of temperature ranging from RT to 10 K for the 6×6 phase (open blue circles), $\beta\sqrt{3}$ phase (open red triangles), and “ 1×1 ” surface (gray crosses). Solid lines on the 6×6 and $\beta\sqrt{3}$ phases are fitting results by Eq. (2) for the low-temperature region. The solid line on the “ 1×1 ” surface is the fitting result by Eq. (1) for the low-temperature region. Dashed lines on the 6×6 and $\beta\sqrt{3}$ phases are fitting results by summing Eq. (1) at the high-temperature region and Eq. (2) at the low-temperature region. The dashed line on the “ 1×1 ” surface is the fitting result by Eq. (1) using different parameters at low-temperature and high-temperature regions. (g) The measured sheet conductivities (σ) as a function of temperature ranging from 250 to 130 K for the 6×6 (open blue squares), $\beta\sqrt{3}$ (open red squares), and the remade 6×6 phases (filled green squares). (h) Sheet conductivity σ of data in (f) on a logarithmic scale as a function of inverse temperature. Solid lines are fitting results by Eq. (1). Dashed lines are eye-guide lines. (i) A magnified graph for the “ 1×1 ” surface. The solid and dashed lines are fitting results by Eq. (1) for low-temperature and high-temperature regions, respectively. (j) Sheet conductivity σ of data in (f) plotted as a function of T (on logarithmic scale). Solid lines are fitting results by Eq. (2).

bending indicates that a pn junction is formed between the surface-space-charge layer (p type) and the underlying bulk (n type), which prevents the measuring current from penetrating into the bulk. Therefore, the experimental measured conductivity is dominated by the surface states.¹³

Previous photoemission spectroscopy (PES) studies show that the surface band structures of both the $\beta\sqrt{3}$ and 6×6 phases are semiconducting, and the bands of the $\beta\sqrt{3}$ phase are simply those of the 6×6 phase with additional broadening.¹⁸ The 6×6 phase exhibits a very sharp 6×6 RHEED pattern [Fig. 1(b)] but the STM image [Fig. 1(a)] shows random arrangements of windmill-like protrusions that correspond to adatoms sitting on some of the 6×6 unit cells.²¹ First-principles calculations show that the energy difference of the 6×6 surfaces with various configurations and numbers of the adatoms is very small,²² implying that the 6×6 phase has the intrinsic defects. The $\beta\sqrt{3}$ phase [Fig. 1(d)] exhibits sharp superlattice spots in RHEED, whereas the direct STM image [Fig. 1(c)] reveals an extremely disordered structure like a glass; however, the Fourier-transformed STM image has sharp $\sqrt{3} \times \sqrt{3}$ spots like the RHEED pattern in Fig. 1(d).

III. RESULTS AND DISCUSSION

Figure 1(f) shows the sheet conductivity (σ) over a wide temperature range for the 6×6 phase, $\beta\sqrt{3}$ phase (made

from the 6×6 phase by thermal quenching), and the “ 1×1 ” surface, all of which have the same Au coverage of nominally 1.0 ML. The conductivities of all three surfaces decrease on cooling below 250 K but with very significant differences. The conductivity of the “ 1×1 ” almost vanishes below 150 K and the other two surface superstructures exhibit much higher conductivities which are as large as the minimum metallic conductivity ($2e^2/h = 77.5 \mu\text{S}$) given by Mott-Ioffe-Regel criterion. The minimum metallic conductivity is a rough criterion dividing weak localization regime ($\sigma \gg 2e^2/h$) and the strong one ($\sigma \ll 2e^2/h$). Under the assumption that localization occurs in these phases, the 6×6 and the $\beta\sqrt{3}$ phases are in the intermediate localization regime between the strong and weak ones in 10–150 K.

The 6×6 phase always has a higher conductivity than the $\beta\sqrt{3}$ phase. As shown in Fig. 1(g), when the 6×6 phase was remade from the $\beta\sqrt{3}$ phase by annealing and slow cooling, the conductivity returned to higher values (filled green squares). Thus, the difference in conductivity between the 6×6 and $\beta\sqrt{3}$ phases is clearly attributable to the crystalline-glass transition of the monolayer¹³ and not due to contamination on the surface.

Figures 1(h) and 1(i) show the log-scale sheet conductivity as a function of inverse temperature for the same data in Fig. 1(f). Different slopes in the high-temperature (dashed lines) and low-temperature (solid lines) regimes are recog-

nizable, indicating a combination of two conduction mechanisms. The black solid lines are fitting results by temperature dependence of hopping conduction between strongly localized states,

$$\sigma = \sigma_0 \exp\left(-\frac{\Delta E}{k_B T}\right), \quad (1)$$

where the prefactor σ_0 and activation energy ΔE are fitting parameters, and k_B is the Boltzmann constant. The obtained values of ΔE are 0.45 meV for the 6×6 phase and 1.1 meV for the $\beta\text{-}\sqrt{3}$ phase. These values are much smaller than the reported band gap ~ 50 meV taken by PES.¹⁸ Therefore, this temperature dependence is not due to semiconducting band conduction.

As shown by dashed lines in Figs. 1(f), 1(h), and 1(i), conductivities in the high-temperature region can be fitted by Eq. (1), giving an activation energy $\Delta E \sim 30$ meV for the 6×6 phase, 70 meV for the $\beta\text{-}\sqrt{3}$ phase, and ~ 180 meV for the “ 1×1 ” surface. Although these values roughly correspond to the band gap observed by PES, the nature of temperature dependences at the high-temperature region is not fully understood. We here focus on the low-temperature region only.

The description of our data in the low-temperature region by strong localization, however, is not unique. The conductivity data of the 6×6 and $\beta\text{-}\sqrt{3}$ phases in this temperature range can be fitted equally well by weak localization theory, as below. Figure 1(j) shows the T (plotted on logarithmic scale) dependence of σ . As shown by the fits to the data in this figure, the conductivities of the 6×6 and $\beta\text{-}\sqrt{3}$ phases can be described also by weak localization theory¹⁻³

$$\sigma = cL_{00} \ln T + \text{const}, \quad (2)$$

where c and const are fitting parameters, $L_{00} = 12.3$ (μS) (quantum conductance divided by 2π). The value of c ($\approx 1-2$) is related to the temperature dependence of the phase relaxation time of carriers. The evaluated c values are reasonable: $c = 1.2$ for the 6×6 phase and $c = 0.84$ for the $\beta\text{-}\sqrt{3}$ phase. These fitting results are also plotted in Fig. 1(f) by solid curves. This picture does not work for the “ 1×1 ” surface at all because $c = 0.26$, far below unity. The character of localization in the 6×6 and $\beta\text{-}\sqrt{3}$ phases now turned out to be an intermediate between strong and weak localizations because both Eqs. (1) and (2) reasonably work with suitable

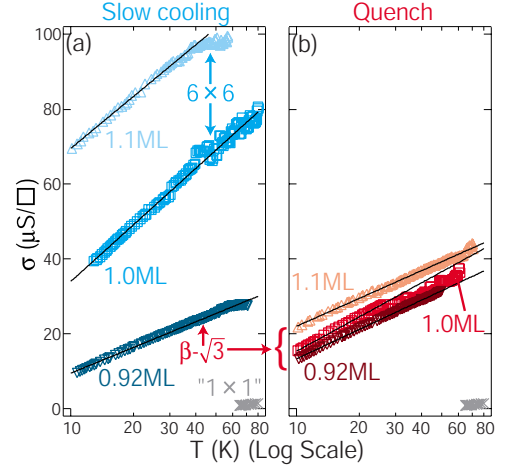


FIG. 2. (Color online) (a) Measured sheet conductivities (σ) plotted as a function of T (on logarithmic scale) over the temperature range from 10 to 80 K, for slowly cooled samples with Au coverages of 0.92, 1.0, and 1.1 ML. (b) Quenched samples with the same Au coverages. Solid lines are fitting results by Eq. (2). The results from the “ 1×1 ” sample are also shown.

parameters in the limited range of temperature. It does not mean that two phases are strongly localized and simultaneously weakly localized. Simply, Eqs. (1) and (2) show almost the same temperature dependence with the chosen parameters in the limited range of temperature.

These analyses indicate that there are localized electronic states at Fermi level (E_F) in both the 6×6 and $\beta\text{-}\sqrt{3}$ phases.¹⁻³ According to the PES results, both the 6×6 and $\beta\text{-}\sqrt{3}$ phases have almost flatbands around 50 meV below E_F .¹⁸ However, the structural disorder may modify the surface states and creates some additional localized states at E_F .

Figure 2 shows the T (plotted on a logarithmic scale) dependence of sheet conductivity for samples with slightly different Au coverages. All of them are well fitted by Eq. (2) with suitable c values as shown by solid lines in Fig. 2 and as listed in Table I. A small increase in the Au coverage leads to a significant increase in the conductivity of samples prepared by slow cooling as shown in Fig. 2(a). The conductivity of the 6×6 phase at 1.2 ML coverage is almost the same as that at 1.1 ML coverage, implying completion of the 6×6 reconstruction at 1.1 ML. The surface with 0.92 ML Au coverage always had a $\beta\text{-}\sqrt{3}$ structure even for samples prepared by

TABLE I. Results of data fitting with Eqs. (1) and (2) c [Eq. (2)] was determined from the data shown in Fig. 2. ΔE and σ_0 [Eq. (1)] were determined from the data of Fig. 3.

Cooling	Coverage	RHEED	c	ΔE (meV)	σ_0 ($\mu\text{S}/\square$)
Slow	0.92	$\beta\text{-}\sqrt{3}$	0.80	1.07	30.8
Slow	1.0	6×6	1.77	0.73	75.0
Slow	1.1	6×6	1.62	0.34	102
Quench	0.92	$\beta\text{-}\sqrt{3}$	0.92	0.87	35.4
Quench	1.0	$\beta\text{-}\sqrt{3}$	1.07	0.84	40.0
Quench	1.1	$\beta\text{-}\sqrt{3}$	0.87	0.55	41.0

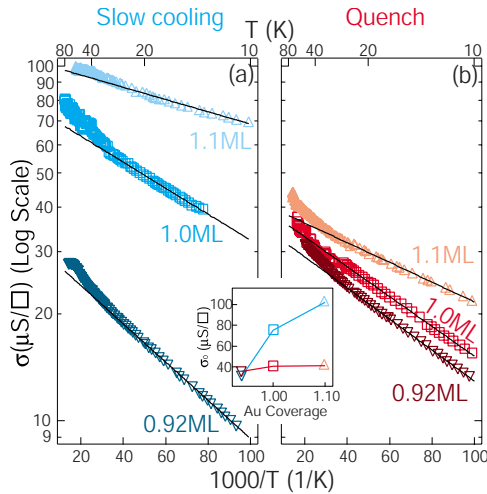


FIG. 3. (Color online) Sheet conductivity σ plotted on logarithmic scale as a function of inverse temperature from 10 to 80 K for the same data as in Fig. 2. Solid lines are the fitting results by Eq. (1) below 25 K. The inset shows the prefactor σ_0 obtained from the fitting.

slow cooling and this phase had a lower conductivity. In contrast, for all of the quenched samples, with the $\beta\text{-}\sqrt{3}$ structure, the conductivity did not depend significantly on the Au coverage as shown in Fig. 2(b). The conductivities of both samples of the $\beta\text{-}\sqrt{3}$ phase with 0.92 ML coverage shown in Figs. 2(a) and 2(b) are quite similar irrespective of the cooling rate.

In Fig. 3, the same data as in Fig. 2 are plotted on a logarithmic scale as a function of inverse temperature. Solid lines are fitting results by Eq. (1) below 25 K, giving the fitting parameters summarized in Table I and inset of Fig. 3. As indicated in Table I, ΔE decreases and σ_0 increases with increase in Au coverage for the slowly cooled surfaces, which correspond to the formation of 6×6 reconstruction. Thus, the degree of disorder in the structure changes the degree of carrier localization. In a weakly disordered system such as the 6×6 phase, the electronic states are less local-

ized. Then the tunneling probability between the two localized sites is larger, resulting in larger σ_0 . In addition, energy differences between the two states tend to be small with better order in the structure, resulting in a smaller activation energy ΔE . In contrast, ΔE and σ_0 do not change so much for the quenched surfaces because the surface structure ($\beta\text{-}\sqrt{3}$) already has strong disorder.

The hopping process described by Eq. (1) is the nearest-neighbor hopping. At sufficiently low temperature, however, the conductivity decreases and may exhibit a temperature dependence of variable-range hopping type. Such a transition from the nearest-neighbor hopping to variable-range hopping conduction was not clearly observed in the present study although some sign for it was observed. It would be interesting to study how the difference of disorder in surface structures affects the nature of hopping conduction in monolayers.

IV. SUMMARY

We have succeeded in detecting a clear difference in the surface electrical conduction between the ordered crystalline 6×6 reconstruction and disordered glassy $\beta\text{-}\sqrt{3}$ reconstruction at the same Au coverage, depending on the degree of structural disorder in the monatomic layer. Compared with the 6×6 phase, the wave functions on the $\beta\text{-}\sqrt{3}$ phase are more strongly localized, causing a larger activation energy and smaller probability of the hopping process, resulting in a lower conductivity. It is also important to mention that the monatomic layers were found to exhibit conductivities as large as the minimum metallic conductivity at the low-temperature region, which meant that metallic (localized) states existed at E_F , in contradiction with PES results.

ACKNOWLEDGMENTS

We thank F. Komori and M. Noda for fruitful discussions. This work was supported by Grants-In-Aid from the Japan Society for the Promotion of Science (JSPS) and Japan Science and Technology Agency, and the A3 Foresight Program by JSPS-KOSEF-NSF.

*yamazaki@surface.phys.s.u-tokyo.ac.jp

[†]Present address: Synchrotron Radiation Laboratory, Institute for Solid State Physics, University of Tokyo, 5-1-5 Kashiwanoha, Kashiwa 277-8581, Japan.

[‡]Present address: Institute of Physics and Applied Physics, and Center for Atomic Wires and Layers, Yonsei University, Seoul 120-749, Korea.

¹P. W. Anderson, Phys. Rev. **109**, 1492 (1958).

²E. Abrahams, P. W. Anderson, D. C. Licciardello, and T. V. Ramakrishnan, Phys. Rev. Lett. **42**, 673 (1979).

³P. A. Lee and T. V. Ramakrishnan, Rev. Mod. Phys. **57**, 287 (1985).

⁴N. F. Mott, J. Non-Cryst. Solids **1**, 1 (1968).

⁵N. F. Mott, Adv. Phys. **21**, 785 (1972).

⁶See <http://www.capres.com>

⁷S. Hasegawa, I. Shiraki, F. Tanabe, R. Hobara, T. Kanagawa, T.

Tanikawa, I. Matsuda, C. L. Petersen, T. M. Hansen, P. Boggild, and F. Grey, Surf. Rev. Lett. **10**, 963 (2003).

⁸T. Tanikawa, I. Matsuda, R. Hobara, and S. Hasegawa, e-J. Surf. Sci. Nanotechnol. **1**, 50 (2003).

⁹T. Kanagawa, R. Hobara, I. Matsuda, T. Tanikawa, A. Natori, and S. Hasegawa, Phys. Rev. Lett. **91**, 036805 (2003).

¹⁰H. Okino, R. Hobara, I. Matsuda, T. Kanagawa, S. Hasegawa, J. Okabayashi, S. Toyoda, M. Oshima, and K. Ono, Phys. Rev. B **70**, 113404 (2004).

¹¹I. Matsuda, M. Ueno, T. Hirahara, R. Hobara, H. Morikawa, C. Liu, and S. Hasegawa, Phys. Rev. Lett. **93**, 236801 (2004).

¹²T. Tanikawa, I. Matsuda, T. Kanagawa, and S. Hasegawa, Phys. Rev. Lett. **93**, 016801 (2004).

¹³S. Yamazaki, I. Matsuda, H. Okino, H. Morikawa, and S. Hasegawa, e-J. Surf. Sci. Nanotechnol. **3**, 497 (2005).

¹⁴J. W. Wells, J. F. Kallehauge, T. M. Hansen, and Ph. Hofmann,

- Phys. Rev. Lett. **97**, 206803 (2006).
- ¹⁵J. Nogami, A. A. Baski, and C. F. Quate, Phys. Rev. Lett. **65**, 1611 (1990).
- ¹⁶D. Grozea, E. Bengu, and L. D. Marks, Surf. Sci. **461**, 23 (2000).
- ¹⁷T. Nagao, S. Hasegawa, K. Tsuchie, S. Ino, C. Voges, G. Klos, H. Pfnür, and M. Henzler, Phys. Rev. B **57**, 10100 (1998).
- ¹⁸H. M. Zhang, T. Balasubramanian, and R. I. G. Uhrberg, Phys. Rev. B **66**, 165402 (2002); **65**, 035314 (2001).
- ¹⁹T. Okuda, H. Daimon, H. Shigekawa, S. Suga, T. Kinoshita, and A. Kakizaki, J. Electron Spectrosc. Relat. Phenom. **80**, 229 (1996).
- ²⁰H. Lüth, *Surface and Interfaces of Solid Materials* (Springer-Verlag, Berlin, 1995).
- ²¹D. Grozea, E. Landree, L. D. Marks, R. Feidenhans'l, M. Nielsen, and R. L. Johnson, Surf. Sci. **418**, 32 (1998).
- ²²M. Noda and S. Watanabe (private communication).